that carriers on these curved surfaces turn through a small angle $\Delta\theta$ in the time τ; consequently, contributions from carriers which cross the boundaries between the flat and curved regions Fermi surface may be neglected. The contributions from the rounded *corners* may also be neglected. The only contribution to the Hall current which needs to be considered is

$$i_{yx} = \left(\frac{4}{h^3}\right)\int_{-\pi/2}^{\pi/2} \{[(2p)(eE\tau)(p_r \cos\theta d\theta)] \times e[v\sin(\theta+\Delta\theta) - v\sin\theta]\}\ , \qquad \text{(A3)}$$

where p_r is the radius of the curved cylindrical surface and $\Delta\theta = evH\tau/p_r$. The three momentum factors in the first square bracket determine the differential volume element of contributing carriers and the second bracket gives the change in their transverse velocity.

The numerical coefficient of Eq. (A3), after integration, is 4π instead of the 8 which was obtained for the sharp-edged cubic [see Eq. (4) of I]. Hence, $r = \frac{1}{4}\pi$ rather than $\frac{1}{2}$.

*Work supported in part by ONR Contract No. PO-9-0163.

[1]R. S. Allgaier, Phys. Rev. 165, 775 (1968), hereafter referred to as I.

[2]E. A. Stern (private communication).

[3]L. Davis, Phys. Rev. 56, 93 (1939).

[4]J. R. A. Cooper and S. Raimes, Phil. Mag. 4, 145 (1959).

[5]R. S. Allgaier, Phys. Rev. 152, 808 (1966).

[6]H. Jones and C. Zener, Proc. Roy. Soc. (London) A145, 268 (1934).

[7]As, for example, in Zn and Cd: see Landolt-Börnstein, *Zahlenwerte und Funktionen* (Springer-Verlag, Berlin, 1959), 6th ed., Vol. 2, Part 6, p. 169.

[8]R. S. Lee and S. Legvold, Phys. Rev. 162, 431 (1967).

[9]A. G. Aronov and P. Kh. Musaev, Fiz. Tverd. Tela 9, 2284 (1967) [Soviet Phys. Solid State 9, 1790 (1968)].

[10]E. A. Stern, *Optical Properties and Electronic Structure of Metals and Alloys* (North-Holland, Amsterdam, 1966), p. 599.

[11]E. A. Stern, Bull. Am. Phys. Soc. 5, 150 (1960); Univ. of Maryland Tech. Report No. 261 (unpublished).

[12]For example, the second band of Al [W. A. Harrison, Phys. Rev. 118, 1190 (1960)] and the hole octahedron of *W* [L. F. Mattheiss, *ibid.* 139, A1893 (1965)].

PHYSICAL REVIEW B VOLUME 2, NUMBER 10 15 NOVEMBER 1970

de Haas–van Alphen Effect in Thallium†

Y. Ishizawa* and W. R. Datars‡
Department of Physics, McMaster University, Hamilton, Ontario, Canada
(Received 13 July 1970)

The de Haas–van Alphen (dHvA) effect in single crystals of high-purity thallium has been investigated in magnetic fields up to 55 kOe. These measurements extend previous work by providing accurate dHvA frequencies for field directions in the three principal crystallographic planes. dHvA frequencies larger than 10^7 G are assigned to orbits on the third-zone hole surface centered at *A* and the fourth-zone hexagonal network of Soven's relativistic orthogonalized-plane-wave model. Comparisons with the single-orthogonalized-plane-wave Fermi-surface model are also made. Magnetic breakdown of some of the orbits is observed. Lower dHvA frequencies are assigned to a small dumbbell-shaped surface with symmetry $\bar{6}m2$. The cyclotron masses of orbits on this surface are also presented and compared with recent cyclotron resonance results.

I. INTRODUCTION

There have been recent investigations of the Fermi surface of thallium using magnetoresistance,[1–5] the magnetoacoustic effect,[6–8] cyclotron resonance,[9,10] and the de Haas–van Alphen (dHvA) effect.[11–16] The dHvA frequency is proportional to the extremal cross-sectional area of the Fermi surface normal to the magnetic field direction. It is therefore important to have complete accurate dHvA measurements as a function of magnetic field direction. They are useful for determining features of the Fermi surface and for deriving the band structure and Fermi surface by the pseudopotential method.

Some high dHvA frequencies were measured by Priestley using pulsed magnetic fields[13] and will be compared with the present results wherever possible. Low dHvA frequencies were observed by the present authors,[14] Anderson, Schirber, and Stone,[15] and Saito.[12] These low-frequency results were extended by Capocci *et al.*[16] and interpreted in terms of a small dumbbell-shaped Fermi surface

located at either H or K in the fifth zone.

The hexagonal Brillouin zone of thallium is shown in Fig. 1. The Fermi surface of thallium has been calculated by the relativistic orthogonalized-plane-wave (ROPW) method[17] and the single-OPW method.

The purpose of the present paper is to provide detailed accurate dHvA frequency measurements of hcp thallium. The experimental method is described in Sec. II. The experimental results of Sec. III consist of high and low dHvA frequencies for magnetic field directions in the three principal crystallographic planes and the cyclotron masses of orbits on the dumbbell Fermi surface. In Sec. IV, the high frequencies are discussed in terms of the third-zone hole surface centered at A and the fourth-zone hexagonal network. The low frequencies are assigned to the dumbbell-shaped Fermi surface in the fifth zone. Comparison of our results to results of other dHvA experiments and to cyclotron masses measured by Azbel'-Kaner cyclotron resonance are also made.

II. EXPERIMENTAL PROCEDURE

Single crystals were made from high-purity Cominco[18] thallium (6N grade) in a sealed evacuated (10^{-6}-Torr) Pyrex tube using a slowly cooling technique. The inside of the tube was coated with carbon obtained by heating benzene. The horizontal furnace was adjusted to provide a temperature gradient of 2 °C/cm along the sample. Thallium in the tube was melted and subsequently cooled through the melting point (303.5 °C) and the bcc-hcp phase transition[19] (230 °C) to room temperature at a rate of 8 °C/h. Samples with approximate dimensions of 3 mm×3 mm×3 mm were cut from a crystal with a spark-erosion machine. Surface damage caused by spark cutting was removed by an etch of dilute HNO_3 and H_2SO_4. Sample orientation was made by the back-reflection Laue method for study with the magnetic field in (0001), $(11\bar{2}0)$, and $(10\bar{1}0)$ planes. The error in orientation of each plane when mounted for measurement was ±0.5°.

The dHvA oscillations were observed using torque and low-frequency field modulation methods. The lowest frequency branch reported for the $(10\bar{1}0)$ and $(11\bar{2}0)$ planes was observed only by the torque method. The (0001) plane was not studied in the usual way by the torque method, so that the very low-frequency oscillations reported recently by Capocci *et al.*[16] were not observed by us. All other dHvA frequencies that are reported were measured by the field modulation method.

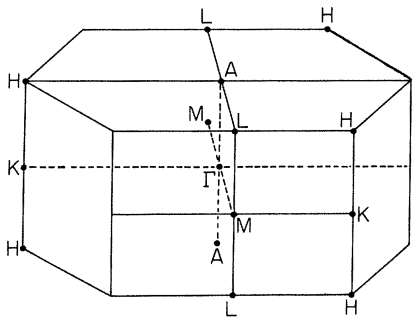

FIG. 1. Brillouin zone for hexagonal-close-packed thallium.

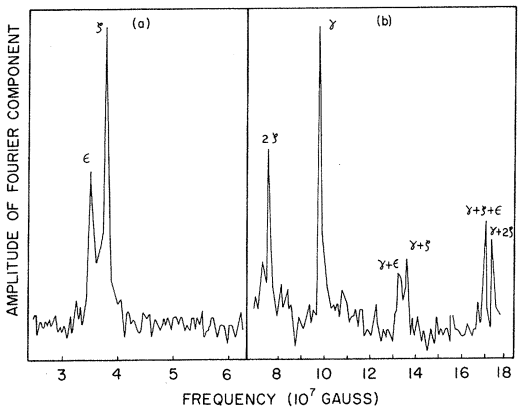

FIG. 2. Fourier transform spectra of dHvA oscillations for the $[10\bar{1}0]$ field direction in thallium: (a) 2.5 to 6.25×10^7 G; (b) 7.0 to 18.0×10^7 G. The ordinate scales in both (a) and (b) are proportional to the square root of the Fourier amplitude. This suppresses dominant peaks and improves the visibility of low-amplitude peaks on one plot.

The torque magnetometer has been described previously.[20] Magnetic fields up to 20 kOe were provided by an electromagnet and measured to an accuracy of 0.1% with a Rawson rotating gaussmeter that had been calibrated by NMR. Data were taken as a function of magnetic field at fixed field direction or as a function of field direction at constant field.

Our field modulation method used the advantages of large amplitude field modulation[21] parallel to the static magnetic field and Fourier transform computer analysis. Details of the method will be published elsewhere.[22] The magnetic field of a niobium-zirconium 55-kOe superconducting magnet was determined with an accuracy of a 0.1% from the field-current relationship that had been calibrated by NMR. Fourier transform spectra for the $[10\bar{1}0]$ field direction are shown in Fig. 2. The field modulation and electronic filtering of the dHvA spectrometer were set to maximize the signal from the ζ orbit in Fig. 2 (a) and the γ orbit in Fig. 2 (b). The fundamental of the ϵ orbit as well as harmonic and sum frequencies are also evident in Fig. 2.

The cyclotron mass was determined for temperatures between 1.1 and 2.1 °K in the usual way from the temperature dependence of the amplitude of

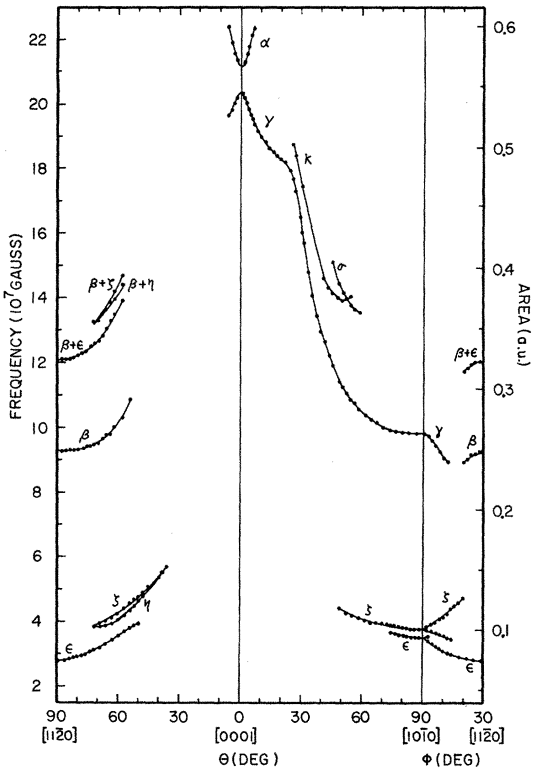

FIG. 3. Observed dHvA frequencies larger than 2×10^7 G in three principal planes of thallium.

dHvA oscillations.

III. EXPERIMENTAL RESULTS

dHvA frequencies larger than 2×10^7 G are shown in Fig. 3 for field directions in the principal crystallographic planes. The fundamental frequency branches α, γ, σ, κ, β, ϵ, ζ, and η are labeled according to the orbit assignments discussed in Sec. IV. The sum frequencies plotted in Fig. 3 will be related to Priestley's results. Many other sum frequencies and harmonics were observed but are not shown in Fig. 3.

The α frequency was observed only within 6° of the (0001) axis. The minimum frequency of this branch is 21.18×10^7 G. The γ frequency was observed for all directions in the $(11\bar{2}0)$ plane, although for $27° < \theta < 32°$ it was only evident in the Fourier transform spectra. The γ frequency was observed only within 6° of the [0001] axis in the $(10\bar{1}0)$ plane. The orbit is expected to exist for larger θ except close to $(11\bar{2}0)$. It probably was not observed in this region because of a large $\partial F/\partial\theta$ which reduces the dHvA amplitude by causing the magnetization vector to be at a large angle to the detection coil axis and permitting small crystalline imperfections to smear out the phase of the oscillations over the sample. In the (0001) plane, the γ frequency decreased as ϕ increased from 0° and disappeared at $\phi = 13°$. This is in contrast to the previous work[13] which reported the γ branch for all directions in the (0001) plane. However, there are two different branches in this region with the β branch existing near the $[11\bar{2}0]$ axis. The β frequency is also observed in the $(10\bar{1}0)$ plane and extends to 36° from the $[11\bar{2}0]$ axis. The frequencies in the (0001) and $(10\bar{1}0)$ planes that are found in the present investigation to be the sum frequency $\beta+\epsilon$ were observed by Priestly.[13] However, he considered them to be fundamentals arising possibly from the β orbit. Our interpretation is supported by the observation of other sum frequencies such as $\beta+\zeta$ and $\beta+\eta$ shown in Fig. 3. The degenerate ζ and ϵ branches in the $(11\bar{2}0)$ plane each split into two branches in the (0001) plane. The cause of the limited range of the ζ branch in the (0001) plane is discussed in Sec. IV. The κ and σ frequencies are assigned to new orbits. The signal strength for the former is rather large and for the latter is very small.

The low-frequency branches are shown in Fig. 4. In the (0001) plane the ξ frequency is constant within experimental error with a value at 4.996×10^6 G. It was observed within 19° of the $[10\bar{1}0]$ axis in the $(11\bar{2}0)$ plane and 17° of the $[11\bar{2}0]$ axis in the $(10\bar{1}0)$ plane. However, it has been shown[16] recently that this branch joins continuously with the ϕ branch, as indicated by the dashed line in Fig. 4. The angular dependence of the ϕ branch from [0001] is the same in $(10\bar{1}0)$ and $(11\bar{2}0)$ planes. There is one ν branch in the $(11\bar{2}0)$ plane, although it splits into two in

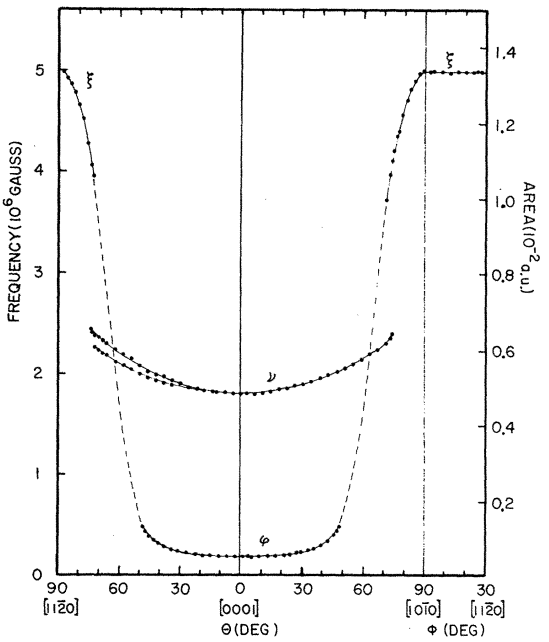

FIG. 4. Observed dHvA frequencies in the low-frequency region in three principal planes of thallium.

planes that are several degrees from $(11\bar{2}0)$. There are two ν branches in the $(10\bar{1}0)$ plane with a frequency difference of 0.12×10^6 G at $\theta=72°$. The ν branch disappears at 74° from the [0001] axis in both $(11\bar{2}0)$ and $(10\bar{1}0)$ planes. There is a strong second-harmonic component of the ν branch. This is the case particularly above 35 kOe at $\theta=40°$ for which the amplitude of the fundamental is 10% of that of the second harmonic. The cyclotron masses of the ϕ and ξ branches are shown in Fig. 5. The frequencies of orbits for certain field directions are given in Table I.

IV. DISCUSSION

A. High dHvA Frequencies

The single-OPW and Soven's ROPW models of hcp thallium are useful in the analysis. Both models give a Fermi surface consisting of sheets scattered throughout the third, fourth, fifth, and sixth zones. However, for the discussion of our high-frequency results, we shall use only the third-zone surface surrounding unoccupied regions of k space centered at point A and the fourth-zone surface enclosing occupied regions of k space. The single-OPW model in the single-zone scheme is shown in Fig. 6. Its third-zone "crown" surface is qualitatively similar to the ROPW third-zone "cookie" surface shown in Fig. 7 (a). The fourth-zone surface of the ROPW model shown in

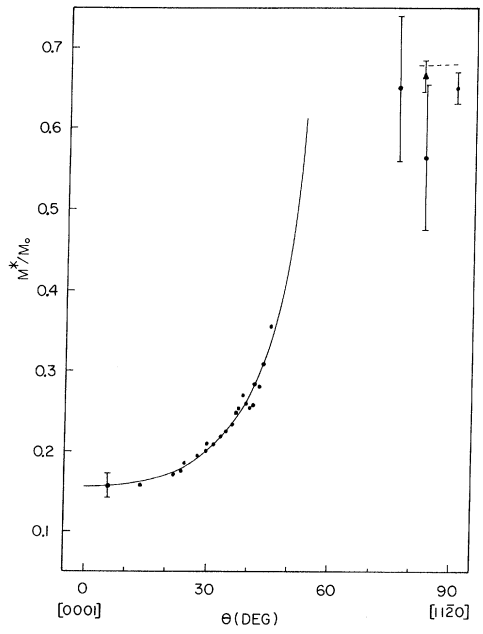

FIG. 5. Cyclotron masses of the ϕ and ξ orbits on the dumbbell-shaped Fermi surface. ● and ▲ show the present results and results by Capocci *et al.*, respectively. The solid line is the S branch and the dashed line is the J branch from the cyclotron resonance measurements by Shaw and Everett.

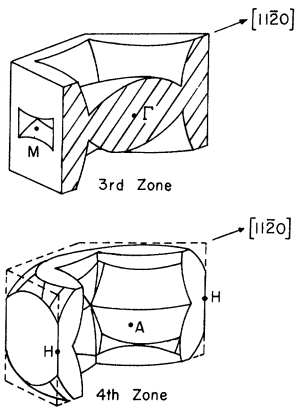

FIG. 6. The single-OPW model in the single-zone scheme of the Fermi surface of thallium in the third and fourth zones.

Fig. 7 (b) forms a hexagonal network of connected arms directed along LHL lines. Twelve posts directed almost parallel to [0001] are attached to the top and bottom of this network near the corners of the zone. In the single-OPW model the arms are qualitatively similar but the posts are connected in the ΓKM plane. The latter feature has been ruled out experimentally.[4]

The areas A of certain orbits on the single-OPW model were calculated using the method of Taylor[23] with lattice constants a = 3.438 Å and c = 5.478 Å of thallium as measured by Barrett[24] at 5 °K. Cross-sectional areas are related to the dHvA frequency F by the Onsager relation:

$$F=c\hbar A/2\pi e=3.741\times10^8\times A\ ,$$

where F is in Gauss and A is in atomic units.

The branch of highest frequency (α branch) is caused by the α orbit which is a hole orbit that goes around the inside of the hexagonal opening of the fourth-zone hexagonal network. Its area is a minimum in the AHL plane and increases rapidly

TABLE I. Some dHvA frequencies of thallium.

Field direction	Band No.	Orbit	Frequency (G)
[0001]	3	γ	$(20.37\pm0.08)\times10^7$
[11$\bar{2}$0]	3	γ	$\sim8.45\times10^7$
[11$\bar{2}$0]	3	β	$(9.31\pm0.03)\times10^7$
[10$\bar{1}$0]	3	γ	$(9.82\pm0.03)\times10^7$
[0001]	4	α	$(21.18\pm0.08)\times10^7$
[11$\bar{2}$0]	4	ϵ	$(2.80\pm0.01)\times10^7$
[10$\bar{1}$0]	4	ζ	$(3.79\pm0.01)\times10^7$
[10$\bar{1}$0]	4	ϵ	$(3.48\pm0.01)\times10^7$
$\theta=60°$ in (10$\bar{1}$0)	4	η	$(4.06\pm0.01)\times10^7$
$\theta=30°$ in (11$\bar{2}$0)	4	κ	$(17.47\pm0.08)\times10^7$
[0001]	5	ν	$(1.806\pm0.010)\times10^6$
[0001]	5	ϕ	$(1.81\pm0.01)\times10^5$
[11$\bar{2}$0]	5	ξ	$(4.994\pm0.015)\times10^6$
[10$\bar{1}$0]	5	ξ	$(4.998\pm0.015)\times10^6$

as the field direction is moved away from the [0001] axis. Thus, the area of 0.566 a.u. was found to increase to 0.599 a.u. at 6° from the [0001] axis beyond which it was not observed in both $(11\bar{2}0)$ and $10\bar{1}0)$ planes.

The γ orbit is about the central section of the third-zone hole surface. The angular dependence of the area of this orbit in the single-OPW model is very similar to the γ branch of the $(11\bar{2}0)$ plane as shown in Fig. 8. This supports the assignment of the γ branch to the γ orbit and shows that the single-OPW model of the third-band crown surface is quite good geometrically and topologically. However, the calculated areas are approximately 15% too large because effects such as spin-orbit coupling which could lower the third-band have not been included. Also, it does not include effects that could round off the sharp corners of the Fermi surface. Soven's calculated values for the [0001]

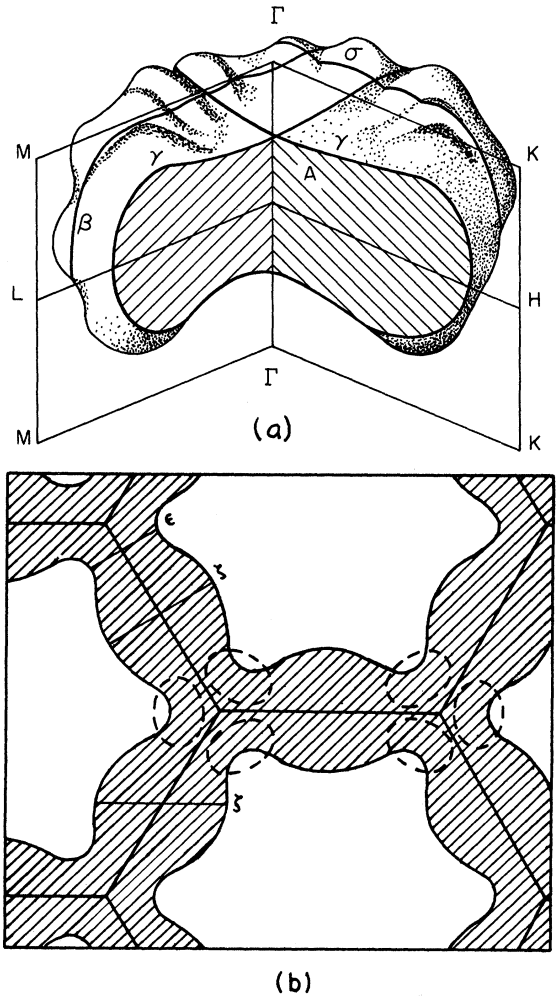

FIG. 7. Relativistic OPW model of thallium: (a) "cookie" surface for third-zone holes; (b) hexagonal network surface in the *AHL* plane for fourth-zone electrons.

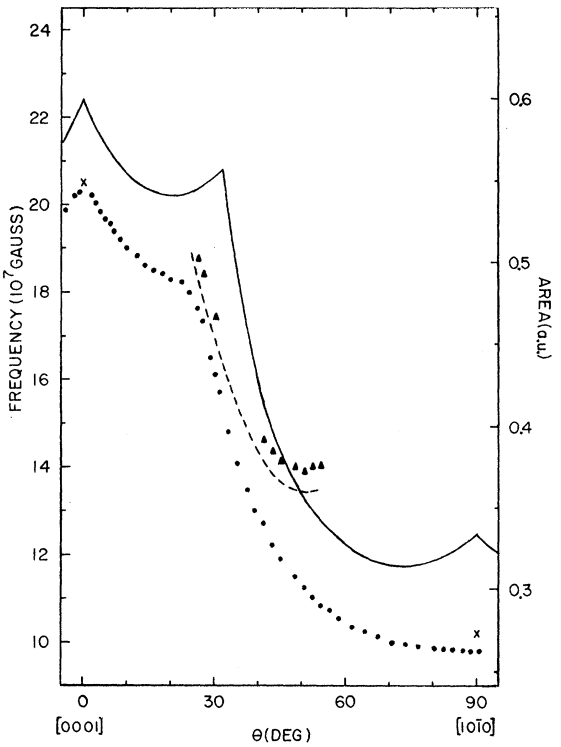

FIG. 8. Comparison of observed dHvA frequencies for γ and κ branches with a single-OPW model. • and ▲ show the observed frequencies for γ and κ branches, respecively. Theoretical angular dependence for γ orbit is shown as a solid line and that of κ orbit as dashed line. x are Soven's calculated frequencies φ for the γ branch.

and $[10\bar{1}0]$ directions are very good, being within 4% of the measured values as shown in Fig. 8. The separation between the third- and fourth-zone bands in the *AHL* plane is caused by spin-orbit coupling.[25] The average value of the energy gap is estimated to be about 0.1 eV from the difference to the area of 0.021 a.u., between the α and γ orbits at the [0001] direction, and is in agreement with that determined previously.[13] The spin-orbit induced gap varies with direction and increases from zero along *AL* to a gap of the order of 0.1 eV along *AH*. Thus, for the $[10\bar{1}0]$ magnetic field direction there is little magnetic breakdown between the third and fourth zones with the magnetic field strengths used in the present experiment. As the energy gap decreases with increasing ϕ, the probability of magnetic breakdown increases. For $13° < \phi \leq 30°$ in Fig. 3, there is magnetic breakdown which results in an open orbit that goes along a $[10\bar{1}0]$ direction[1-4] and there are few central orbits on the third-zone surface (γ orbit) or on the arms of the fourth-zone hexagonal network (ζ orbit). In the $(10\bar{1}0)$ plane, the γ orbit is expected to exist beyond $\theta = 6°$ until it is eliminated by magnetic breakdown when the field is close to the $[11\bar{2}0]$

axis.

The β branch in the (0001) plane does not come from the γ orbit because the angular dependence of the β branch differs from the expectation of the single-OPW model and the γ orbit should disappear near the $[11\bar{2}0]$ axis by magnetic breakdown. The β orbit is a noncentral orbit of the third-zone hole surface, as shown in Fig. 7 (a). This extremal orbit exists for $20° < \phi < 30°$ in the (0001) plane and $0° \leq \theta < 36°$ in the $(10\bar{1}0)$ plane. It does not suffer magnetic breakdown to the fourth zone.

The arms of the fourth-zone hexagonal network support the ϵ, ζ, and η orbits, as illustrated in Fig. 7 (b) and Fig. 9 (a). The ϵ orbit occurs at a minimum extremal area at a noncentral section of the arm. Thus, the lowest frequency branches in the (0001) and $(11\bar{2}0)$ planes are assigned to the ϵ orbit, as Priestley pointed out. It is not affected by magnetic breakdown so that it exists for field directions in the (0001) plane within $\pm 33°$ of the direction of an arm. The ϵ branch in the $(11\bar{2}0)$ plane arises from orbits on the two arms that are at equal angles to the magnetic field. The ζ orbit is a central section of an arm of the hexagonal network (centered at L). The ζ branch is doubly degenerate in the $(11\bar{2}0)$ plane and splits into two in the (0001) plane. The lower branch in the (0001) plane disappears at $\phi = 13.5°$, where there is an open orbit caused by magnetic breakdown between the third and fourth zones. The other branch is cut off at $\phi = 20°$ by the disappearance of the extremal orbit. The ζ orbit is also missing for $\phi < 18°$ in the $(10\bar{1}0)$ plane because of magnetic breakdown. Two close frequency branches are observed between 36° and 72° in the $(10\bar{1}0)$ plane. The higher branch is assigned to the ζ orbit because extrapolation to the $[11\bar{2}0]$ direction gives the same area (0.09 a.u.) for it and for the lower ζ branch in the (0001) plane. Also, the angular dependence is similar to the ϵ branch which is expected for the ζ branch. The branch just below the ζ branch in the $(10\bar{1}0)$ plane is assigned to the η orbit which goes around the arm and posts of the fourth-zone hexagonal network, as shown in Fig. 9 (a). The area of the η orbit predicted by the single-OPW model at $\theta = 60°$ is 0.118 a.u., which may be compared with the measured value of 0.109 a.u.

The κ orbit is on the fourth-zone hexagonal network as shown in Fig. 9 (b). It also exists on the ROPW Fermi surface. The assignment of this orbit to the κ branch is supported by the comparison of calculated and observed extremal areas shown in Fig. 8. Also, Coon *et al.*[8] measured a large caliper with the magnetic field in the range $20° < \theta < 25°$ in the $(11\bar{2}0)$ plane and $\vec{q}$ in the $[11\bar{2}0]$ direction which might be relevant to the κ orbit. The single-OPW model predicts a caliper for this orbit of 1.83×10^8 cm^{-1} at a field direction of $\theta = 25°$, which is in good agreement with their observation.

The assignment of the σ branch in the $(11\bar{2}0)$ plane is very tentative. However, it may be caused by a noncentral orbit of the third-zone surface judging from its angular dependence and area size.

A summary of extremal areas in the third-zone and fourth-zone surfaces for certain field directions

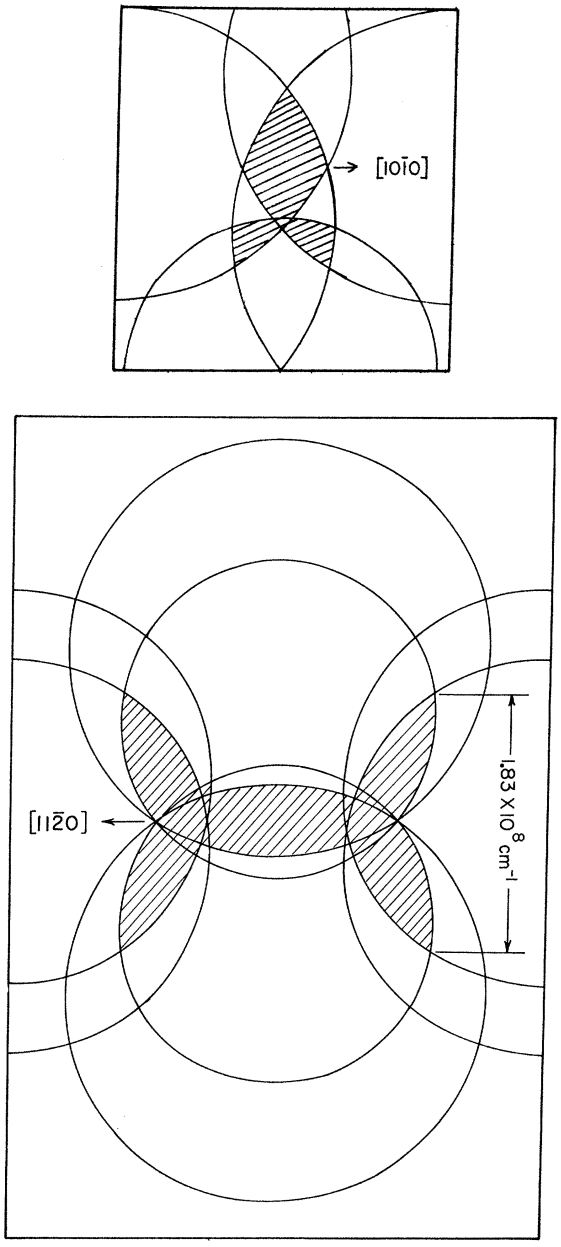

FIG. 9. Extremal orbit shapes for η and κ orbits on the fourth-zone hexagonal network of the single-OPW model: (a) η orbit for the magnetic field direction along $\theta = 60°$ in the $(10\bar{1}0)$ plane; (b) κ orbit for the magnetic field direction along $\theta = 25°$ in the $(11\bar{2}0)$ plane.

TABLE II. Comparison of dHvA areas with theories.

Field direction	Band No. & orbit	Experimental area in a. u. Present data	Priestley [a]	Anderson *et al.* [b]	Theoretical area in a. u. Single OPW	Soven [c]
[0001]	3γ	0.544	0.546	0.544	0.599	0.548
$[11\bar{2}0]$	3β	0.249	0.245	~0.249	0.314	0.275
$[10\bar{1}0]$	3γ	0.262	0.262	···	0.334	0.273
[0001]	4α	0.566	0.571	0.565	0.599	0.582
$[11\bar{2}0]$	4ϵ	0.075	0.075	0.075	0.058	0.069
$[10\bar{1}0]$	4ζ	0.101	0.101	···	0.095	~0.12
$[10\bar{1}0]$	4ϵ	0.093	···	···	···	···
$\theta = 60°$ in $(10\bar{1}0)$	4η	0.109	···	···	0.118	···
$\theta = 30°$ in $(11\bar{2}0)$	4κ	0.467	···	···	0.453	···

[a] M. G. Priestley (Ref. 13)
[b] J. R. Anderson *et al.* (Ref. 15).
[c] P. Soven (Ref. 17).

is given in Table II.

B. Low dHvA Frequencies

The low frequency branches shown in Fig. 4 can be fitted to a dumbbell-shaped Fermi surface with principal axis along the [0001] axis centered at either H or K in the fifth zone, as proposed by Capocci *et al.*[16] The ϕ orbit is about the hyperbolic neck. The two ν branches in the $(10\bar{1}0)$ plane shown in Fig. 4 arise from orbits on the upper and lower lobes. These branches are degenerate in the $(11\bar{2}0)$ plane because the $(10\bar{1}0)$ plane through H or K is a mirror plane. The ξ orbit is around the dumbbell for field directions in the (0001) plane. A cross section shown in Fig. 10 may be constructed from radii derived from extremal areas assuming a surface of revolution about the [0001] axis. The neck and lobes are constructed from the ϕ and ν orbits assuming hyperbolic and ellipsoidal shapes, respectively, and are positioned to join smoothly together. The area of this cross section is 1.34×10^{-2} a.u. and is in very good agreement with the value 1.335×10^{-2} a.u. derived from the ξ branch in the (0001) plane. This was found at an early stage of our work and suggested that the low-frequency orbits are on a dumbbell surface. However, there was not the required continuous variation from the ϕ branch to the ξ branch in our data. This has been observed by Capocci *et al.*[16] They also explained that it is possible for the ϕ and ν branches to cross at $\theta = 63°$ rather than merging. The shape shown in Fig. 10 is approximate. However, deviation from the real shape may be small because of the good agreement between the estimated and measured area and the constant ξ frequency in the (0001) plane. There are a few magnetoacoustic measurements relative to the dumbbell surface. Rayne[6] and Coon *et al.*[8] observed a caliper of 0.07×10^{8} cm^{-1} which is the radius of the lobe in the (0001) plane.

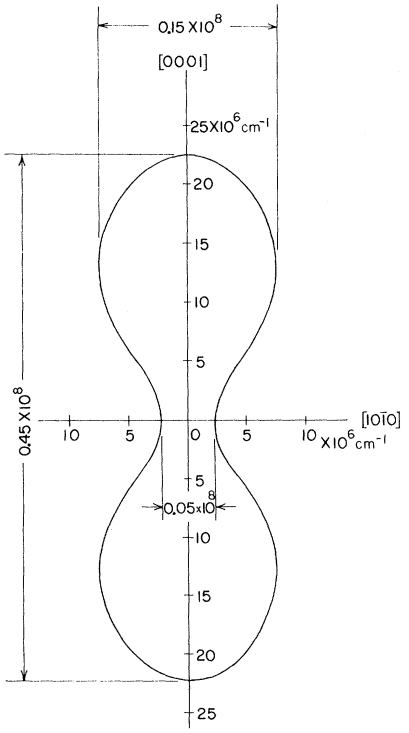

FIG. 10. Cross section in the $(11\bar{2}0)$ plane of the dumbbell Fermi surface.

Figure 5 shows the cyclotron mass of the ϕ and ξ orbits. The cyclotron mass of the ϕ orbit is in good agreement with the mass branch S of Shaw and Everett,[10] thereby giving the assignment of branch S to the ϕ orbit. Mass branch J measured by cyclotron resonance can be assigned to the ξ orbit from the comparison shown in Fig. 5. Our measurements of cyclotron mass also indicate that the D', D'', and N mass branches measured

by Shaw and Everett can be assigned to the ν orbit of the dumbbell-shaped Fermi surface.

V. SUMMARY

Detailed measurements of the dHvA effect in thallium have been made using torque and field modulation methods in magnetic fields up to 55 kOe. The results may be divided into sets of low frequencies and high frequencies. Soven's ROPW model of the third-zone hole surface centered at A and the fourth-zone hexagonal network satisfactorily explain the high frequencies when magnetic breakdown between the third and fourth zones is included. The magnetic breakdown occurs between the central sections of the third- and fourth-zone surfaces for field directions in the region of $[11\bar{2}0]$. This dHvA experiment shows three extremal orbits (γ, β, and σ) on the third-zone Fermi surface and five extremal orbits (α, κ, ξ, ϵ, and η) on the fourth-zone hexagonal network. There are no observations of the Fermi surface at M in the third zone and the electron surface in the sixth zone, which are predicted by both the single-OPW and ROPW models. The low dHvA frequencies are assigned to a dumbbell-shaped Fermi surface located at H or K in the fifth zone.

ACKNOWLEDGMENT

We wish to thank A. Dunsworth for assistance with the Fourier analysis of dHvA oscillations and C. Verge for improving the dHvA apparatus.

---

†Research for this paper was supported by the Defense Research Board of Canada, Grant No. 9510-36.

*Present address: National Institute for Researches in Inorganic Materials, Honkomagome 2-29-3, Bunkyo-ku, Tokyo, Japan.

‡E. W. R. Steacie Research Fellow of the National Research Council.

[1]N. E. Alekseevskii and Yu. P. Gaidukov, Zh. Eksperim. i Teor. Fiz. 43, 2094 (1962)[Soviet Phys. JETP 16, 1481 (1963)].

[2]A. R. Mackintosh, L. E. Spanel, and R. C. Young, Phys. Rev. Letters 10, 434 (1963).

[3]J. C. Milliken and R. C. Young, Phys. Rev. 148, 558 (1966).

[4]R. C. Young, Phys. Rev. 163, 676 (1967).

[5]R. E. Hamburg, C. G. Grenier, and J. M. Reynolds, Phys. Rev. Letters 23, 236 (1969).

[6]J. A. Rayne, Phys. Rev. 131, 653 (1963).

[7]Y. Eckstein, J. B. Ketterson, and M. G. Priestley, Phys. Rev. 148, 586 (1966).

[8]J. B. Coon, C. G. Grenier, and J. M. Reynolds, J. Phys. Chem. Solids 28, 301 (1967).

[9]W. L. Dahlquist and R. G. Goodrich, Phys. Rev. 164, 944 (1967).

[10]J. C. Shaw and G. E. Everett, Phys. Rev. B 1, 537 (1970).

[11]D. Shoenberg, Phil. Trans. Roy. Soc. A245, 1 (1952).

[12]Y. Saito (unpublished).

[13]M. G. Priestley, Phys. Rev. 148, 580 (1966).

[14]Y. Ishizawa and W. R. Datars, Phys. Letters 30A, 463 (1969).

[15]J. R. Anderson, J. E. Schirber, and D. R. Stone, *Colloque International sur les Propriétés Physiques des Solids sous Pression* (Editions du Centre National de la Recherche Scientifique, Grenoble, 1970), p. 131.

[16]F. A. Capocci, P. M. Holtham, D. Parsons, and M. G. P. Priestley, J. Phys. C 3, 2081 (1970).

[17]P. Soven, Phys. Rev. 137, A1706 (1965); 137, A1717 (1965).

[18]Consolidated Mining and Smelting Company.

[19]*Metals Reference Book*, edited by C. J. Smithells (Butterworths, London, 1962).

[20]J. Vanderkooy and W. R. Datars, Phys. Rev. 156, 671 (1967).

[21]R. W. Stark and L. R. Windmiller, Cryogenics 8, 272 (1968).

[22]R. G. Poulsen, J. Moss, and W. R. Datars Phys. Rev. (to be published).

[23]Roger Taylor, Can. J. Phys. 14, 1403 (1968).

[24]C. S. Barrett, Phys. Rev. 110, 1071 (1958).

[25]L. M. Falicov and M. H. Cohen, Phys. Rev. 130, 92 (1963).